RSC Advances

PAPER

View Article Online
View Journal | View Issue

Cite this: *RSC Adv.*, 2024, **14**, 30518

Evaluation and mechanistic analysis of the effect of the addition of alkaline earth metal CaO on Cd solidification enhancement in lightweight aggregate preparation†

Xin Gao,[a] Shouwei Jian, *[a] Yuting Lei,[a] Baodong Li,[b] Jianxiang Huang,[a] Xiaoyao Ma[a] and Xinxin He[a]

The volatilization of Cd during the preparation of lightweight aggregates (LWAs) can cause serious damage to the environment, so a method to harmlessly transform Cd during this process is required. In this regard, the alkaline earth metal CaO was added to Cd-containing aggregate raw materials for treatment, and the effect of CaO addition on the properties of LWAs in the presence of chlorine and sulfate was investigated. Kinetic models of the Cd volatilization were established by using the Arrhenius equation to predict the volatilization of Cd at different sintering stages. The results showed that 0.8% wt of CaO under the influence of chlorine can reduce the Cd volatilization rate from 84.9% to 12.64%, corresponding to an increase in the reaction activation energy (E_a) from 22.62 to 49.55 kJ mol^{-1}. Additionally, the Cd volatilization rate under the influence of sulfate was reduced from 30% to 8%, with an increase in the E_a from 33.25 to 42.62 kJ mol^{-1}. The activation energy increase suggests that the addition of CaO is beneficial because it increases the energy required for Cd volatilization. According to the Cd leaching experiments conducted on the LWAs, it was found that the solidification ratio of Cd was higher than 99.9% for all samples after the addition of CaO. The addition of CaO promotes the formation of $CdFe_2O_4$ and anorthite for effective solidification of Cd, thus optimizing the structures of the LWAs. This work may provide a new idea for Cd waste recycling.

Received 24th June 2024
Accepted 8th September 2024

DOI: 10.1039/d4ra04610b

rsc.li/rsc-advances

1 Introduction

With technological innovation comes the establishment of more chemical, mining or smelting plants that are periodically renewed, and thus a large amount of heavy metal contaminated soil remains on the original sites of these factories.[1–4] Cadmium (Cd) is a typical volatile metal with a high concentration in contaminated soil,[5,6] which can cause devastating damage to the environment and is harmful to human health.[7,8] Consequently, treatments of heavily Cd-contaminated soil have become a crucial challenge in both industrial and urban development.[9,10] Typical methods for treating heavy metal-contaminated soil include landfill, chemical remediation, and soil improvement, which always cost a lot or easily cause secondary pollution.[11–13] Thermal treatment has been proven to be effective for the harmless disposal of Cd-contaminated solid waste.[14,15] The incorporation of the Cd-containing waste solids into building materials by thermal treatment for added value can significantly contribute to the sustainable development of green technology.[16,17]

Lightweight aggregates (LWAs) are a kind of building support material that are widely used in the construction industry.[18] Utilizing Cd-contaminated soil to produce LWAs for resource utilization is acceptable because the main components in polluted soil are Al_2O_3 and SiO_2.[19–21] However, the volatility of Cd at high temperatures constrains the development of the technology, especially because in the complex composition of solid waste chlorine, sulphur and other active non-metallic elements are present, which has a significant impact on the volatilization of Cd.[22] The presence of sulfur and chlorine is the main factor influencing the volatilization rate of Cd at high temperature during sintering,[23–25] and the volatile Cd compounds produced could cause secondary pollution.[26,27] Therefore, it is necessary to figure out methods to solve the Cd volatilization problem during the process of utilizing Cd-contaminated soil. To further enhance the solidification of Cd, treatments including alkali activation, carbon activation, and binder stabilization can transform the volatile Cd compounds to a stable form. However, these reactions in LWAs always proceed under conditions that require higher contents of

[a]State Key Laboratory of Silicate Materials for Architectures, Wuhan University of Technology, Wuhan, Hubei 430070, China. E-mail: jianshouweiwhut@163.com
[b]Department of Architecture and Civil Engineering, Chalmers University of Technology, 41296 Gothenburg, Sweden

† Electronic supplementary information (ESI) available. See DOI: https://doi.org/10.1039/d4ra04610b

silica, alumina, and calcium, not only to solidify the heavy metals, but also to enhance the performance of the LWAs. Compared to alkali activation, the alkaline earth metals tend to lose electrons in mild chemical reactions by forming cations with strong reducing properties which have been shown to be effective in reducing heavy metals.

The addition of small amounts of cheap alkaline earth metal admixtures directly to the raw materials used in LWAs preparation has a great role in the utilization of contaminated soils in practical engineering. The best way to control the efficiency and the mechanism by which Cd is solidified by alkaline earth metals at high temperature are not understood. Therefore, optimizing the preparation process is important to improve the Cd solidification efficiency. CaO is as a common alkaline earth metal with a wide range of sources and a low cost.[28] CaO is the main active ingredient reported for reactions with chlorides and sulfates to improve the solidification of heavy metals by generating rigid stable structures and glass phases at high temperatures due to the presence of Ca^{2+}.[29–32]

Herein, we prepared LWAs from Cd-contaminated soil and we chose lithium slag as a fluxing agent, whilst CaO was added to solidify the Cd *via* the influence of chlorides and sulfates. The solidification of Cd was evaluated according to the volatilization rate and the solidification ratio of Cd.[33–36] The Arrhenius equation was used to establish kinetic models of the Cd volatilization during sintering process and to predict the volatilization rate of Cd effectively. The mechanism by which CaO enhances the Cd solidification ratio was probed further using the results of the XRD phase composition and XPS microscopy analysis. The effect of CaO on the physical properties of the LWAs was systematically studied and the mechanism of Cd volatilization control by the CaO under the influence of sulfur chloride was also analyzed.[37,38] The results of this work will hopefully provide valuable guidance for the safe treatment and utilization of Cd-contaminated waste solid resources.

2 Experimental

2.1 Materials

The contaminated soil (CS) raw materials were taken from Hubei China, and the lithium slag (LS) was obtained from Jiangxi, China. The chemical compositions of the CS and LS are shown in the ESI (Table S1a and Fig. S1).† $Cd(NO_3)_2 \cdot 4H_2O$ was used as the Cd source. KCl and Na_2SO_4 were used as the sources of chlorine and sulphur, respectively, and were purchased from Sinopharm Chemical Reagent Co., Ltd, China. All agents were of analytical grade and were used without any further treatment. For other chemical reagents not mentioned in this work but still used, refer to the noted literature.[39–41]

2.2 Preparation of the LWAs

Based on previous studies, the mass ratio of the CS to LS was fixed at 9 : 1. The $Cd(NO_3)_2 \cdot 4H_2O$ was added to the CS to simulate Cd-contaminated soil, and the content was 2 wt% of CS. The contents of KCl and Na_2SO_4 were 1 wt% of CS. Additionally, the addition of CaO to solidify specific amounts of Cd are shown in Table S2,† and the CaO control LWAs are denoted as Cl-LWAs-*x*/S-LWAs-*x* (the *x* is the content of CaO). The LWA preparation process is illustrated in detail in Scheme 1. First, the raw pellets are formed by mixing the Cd-contaminated CS, LS and CaO to obtain a uniform mixture, then a solution containing either KCl or Na_2SO_4 was added. The mixed slurry was aged for 2 hours and divided into pellets, each with a mass of 4 g, and the raw pellets were dried at 105 °C for 24 hours. Finally, the dry pellets were sintered at 1100 °C for 20 min with a heating rate of 9 °C min^{-1}. The Cd content of the obtained LWAs was determined after sintering using ICP-OES.

The LWAs for the numeric simulation of the volatilization kinetics were prepared following the same process described above but with a different sintering schedule. The sintering temperature ranged from 200 to 1200 °C with a temperature gradient of 100 °C. The Cd volatilization of the LWAs at each sintering temperature after holding for 6, 12, 18, 24, and 30 minutes was measured.

2.3 Characterization

The specific details of the characterization techniques and processes are described in the ESI.†

3 Results and discussion

3.1 Physical properties analysis

To illustrate the effect of different CaO contents on the LWAs, the bloating index (BI), the water absorption, density and single particle compressive strengths (SPCS) were determined. As shown in Fig. 1(a), when the CaO content increased from 0.2% to 1.0%, the BI of the Cl-LWAs-*x* showed a continuous decrease, and when the CaO content exceeds 0.4% volume shrinkage of the LWAs appears, indicating the structural influence that CaO has on the Cl-LWAs. However, the volume first increased and then decreased and the maximum expansion rate was 22.45% when the CaO content was 0.4% in the S-LWAs-*x*, this shows that CaO has a different effect on the Cl-LWAs-*x* and the S-LWAs-*x*. Furthermore, the density, water absorption and compressive strength of the single particles (SPCS) were also tested. It was found that the density of the Cl-LWAs-*x* increases from 1.196 to 1.500 g cm^{-3}, while the water absorption decreases from 0.62% to 0.32%. The density and water absorption of the S-LWAs-*x* also first decreases and then increases, with a minimum density and absorption of 0.87 g cm^{-3} and 0.86%, respectively (Fig. 1(b)). The density and water absorption changes are in accordance with the change of BI, where a greater volume change corresponds to lower water absorption and higher density. This finding might be due to a change of the pore structure of the LWAs. The SPCS results have a good correlation with the density of the LWAs (Fig. 1(c)). A higher density corresponds to a higher SPCS, and the enhancement of SPCS implies that the addition of CaO can improve the mechanical properties. The maximum values were 6.11 and 8.416 MPa for the Cl-LWAs-*x* and S-LWAs-*x*, respectively.

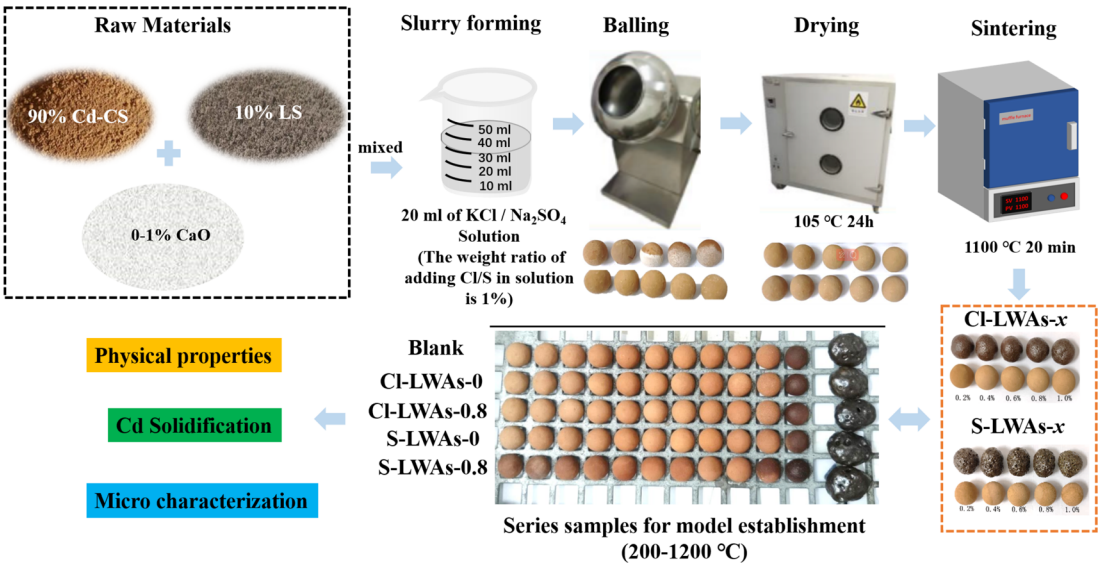

Scheme 1 Schematic diagram of the LWAs preparation process.

3.2 Cd volatilization analysis

The Cd volatilization rates of the different LWAs were determined. Fig. 2(a) and (b) show the change of volatilization rate of Cl-LWAs-*x* and S-LWAs-*x*, respectively, at different levels of added CaO. As the CaO content increased, the Cd volatilization rate of the Cl-LWAs-*x* decreased from 84.90 to 12.64%. This

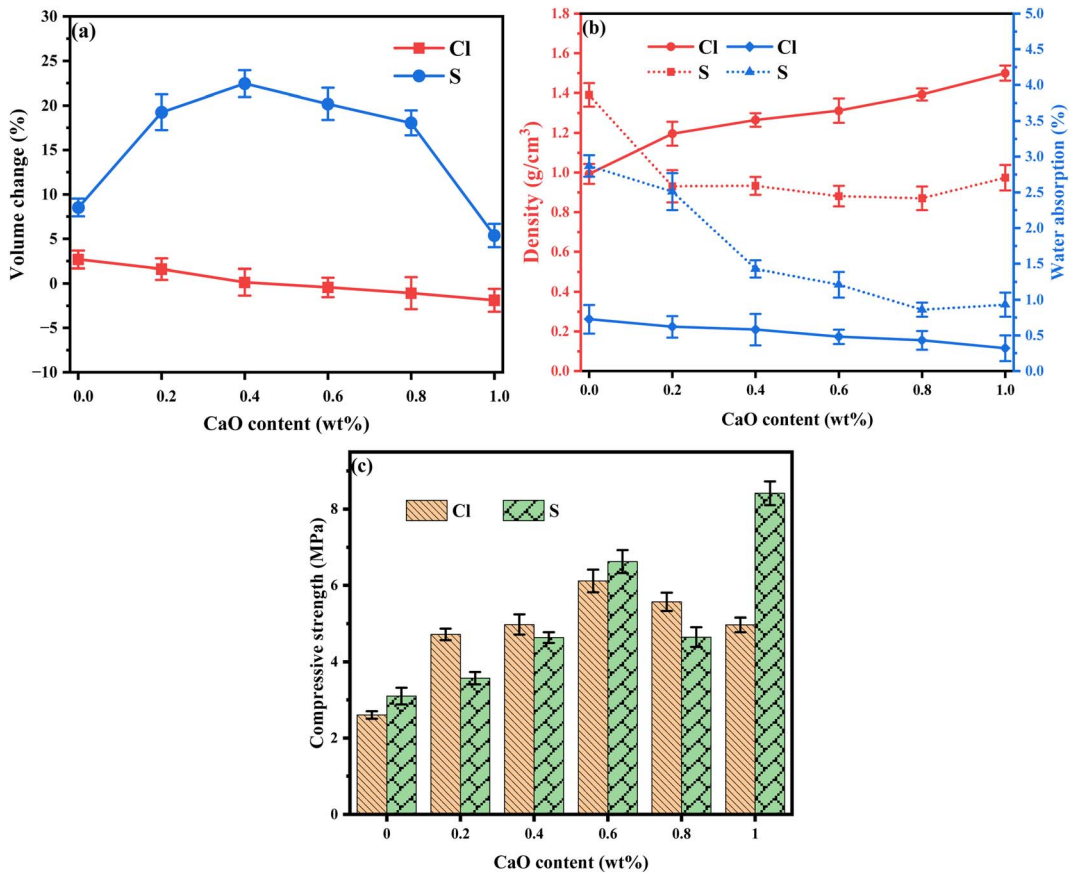

Fig. 1 Effect of different CaO contents on (a) volume change, (b) density and water adsorption and (c) the single-particle compressive strength of the LWAs.

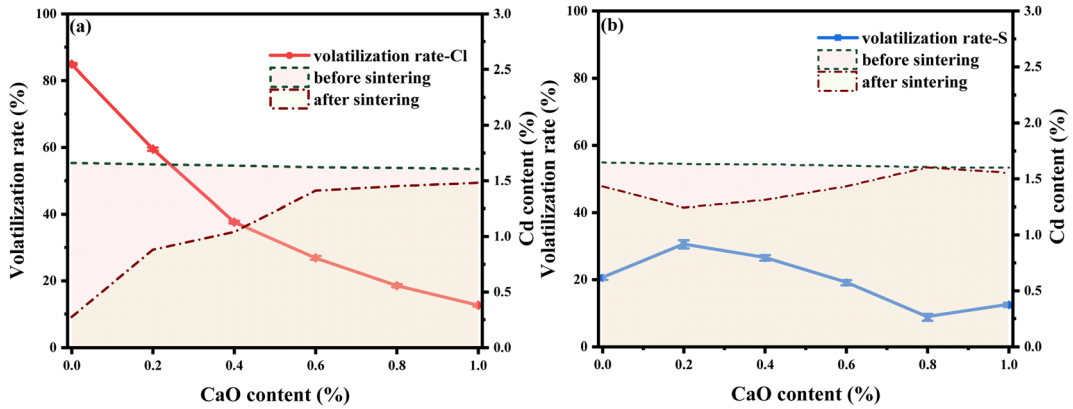

Fig. 2 Cadmium volatilization rate of (a) Cl-LWAs-*x* and (b) S-LWAs-*x* at different CaO contents.

Table 1 Values of the main factor of the kinetic models of the LWAs

Samples	Slope	Intercept	R^2	E_a (kJ mol^{-1})	A (min^{-1})
Cl-LWAs	−2725.5	−5.707	0.90267	22.66	0.047
Cl-LWAs-0.8	−5960	−2.37867	0.92534	49.55	0.6027
S-LWAs	−3998.7	−4.62055	0.98457	33.25	0.1585
S-LWAs-0.8	−5126.3	−3.45533	0.97091	42.62	0.3717

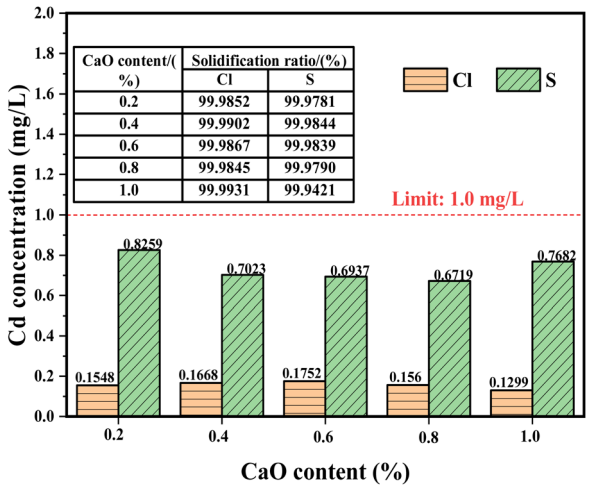

Fig. 3 The leaching concentration and Cd solidification ratio in the LWAs.

decrease of the volatilization rate means that the CaO has greatly aids the solidification of the Cd in the presence of chlorine. However, for the S-LWAs-*x* (Fig. 2(b)), the Cd volatilization rate first increases then decreases, and the Cd volatilization rate is 30.52% and 26.46% when the content of CaO is 0.2% and 0.4%, respectively. As the CaO addition continues to increase the lowest Cd volatilization value achieved was 8.73% at a content of 0.8% of CaO. Therefore, combining the Cd volatilization efficiency with the physical properties of the LWAs and the effect that the CaO content has on the S-LWAs, a CaO content of 0.8% is optimal for controlling the Cd volatilization and was therefore chosen as the optimum content for the next experimental tests. In addition, the Cd volatilization is found to be consistent with the change rule of the physical properties of the LWAs, indicating that the addition of a suitable level of CaO can also optimize the structures of the LWAs.

3.3 Kinetic model analysis

To determine the influence that the addition of CaO has on the rate of reaction of Cd volatilization during sintering, the Arrhenius equation was used to manifest the exponential change of the Cd volatilization rate with temperature and guided a series of experiments to test the Cd volatilization. The relationship between the Cd volatilization rate and the LWA sintering reaction time can be expressed as eqn (1),

$$\frac{dH}{dt} = k(1-H)^n \quad (1)$$

where H is the volatilization rate (%) of Cd, t is the holding reaction time at different temperatures (min), k is the reaction constant, and the reaction order n is 1 in the solid-state volatilization.

From eqn (1), the correlation of the reaction constant k with temperature T can be described by eqn (2).

$$\frac{d\ln k}{dT} = \frac{E_a}{RT^2} \quad (2)$$

where E_a (kJ mol^{-1}) is the activation energy of the reaction, R is the universal gas constant of 8.314 J mol^{-1} K^{-1}, and T (K) is the sintering insulation temperature. The k values can be obtained by integrating eqn (2), as is shown in eqn (3).

$$k = A\exp\left(-\frac{E_a}{RT}\right) \quad (3)$$

where A (min^{-1}) is the frequency factor. Therefore, the reaction rate can be represented by eqn (4), and the volatilization rate H can also be calculated through integral fitting, as shown in eqn (5).

$$\frac{dH}{dt} = A\exp\left(-\frac{E_a}{RT}\right)(1-H)^n \quad (4)$$

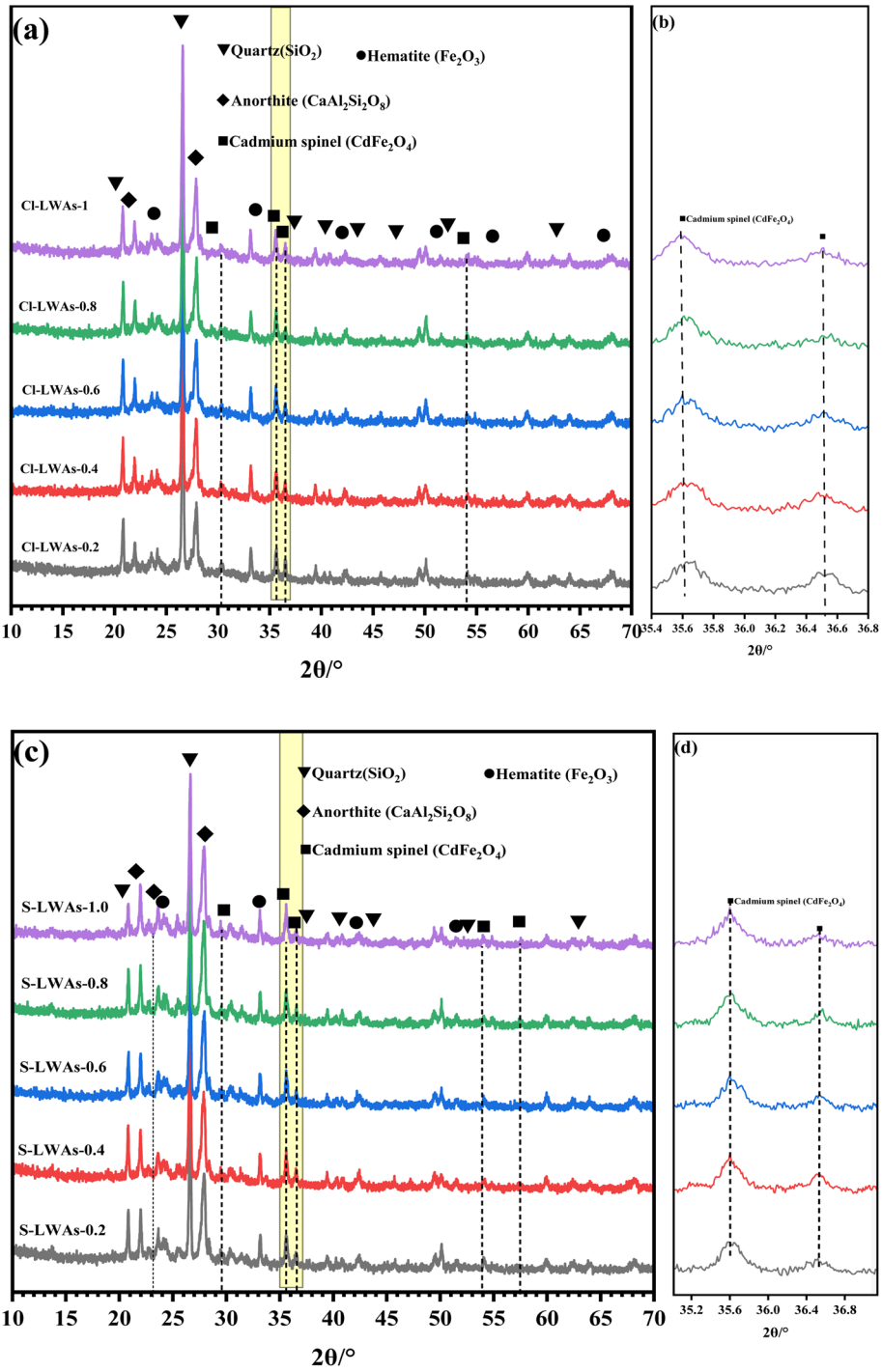

Fig. 4 XRD patterns of (a and b) Cl-LWAs-*x* and (c and d) S-LWAs-*x* with different CaO contents.

$$H = 1 - \exp\left(-A\exp\left(-\frac{E_a}{RT}\right)t\right) \quad (5)$$

The reaction constant k value is linearly fitted to eqn (6) by integrating eqn (1), and the determination coefficient R^2 is obtained based on the linear fitting results.

$$-\ln(1-H) = kt \quad (6)$$

By logarithmic processing of eqn (6), the activation energy E_a and frequency factor value A can be obtained using $1/T$ and $\ln k$ for linear fitting (eqn (7)).

$$\ln k = -\frac{E_a}{RT} + \ln A \quad (7)$$

The activation energy (E_a) and temperature (T) can be calculated to determine the reaction rate constant k,[42] and the

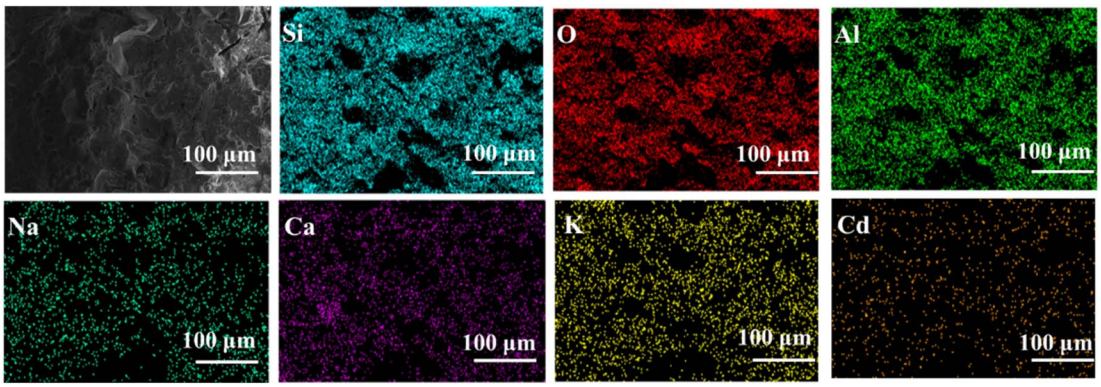

Fig. 5 The SEM image and the corresponding EDS mapping of the elements in Cl-LWA-0.8.

kinetic models of H can be established. The experimentally obtained H values are specified in the ESI.†

Kinetic models were established based on the Cd volatilization rates at different stages. As is shown in Fig. S2(a),† the Cd volatilization rate of Cl-LWAs-0 was measured, and the kinetic model was fitted with a sintering temperature range from 500 to 1200 °C with different holding times. The fitted results are shown in Table S2† and the correlation coefficient value (R^2) is 0.90267 which indicates a great accuracy. Moreover, Fig. S2(b)† shows the correlation of ln k with the inverse value of the sintering temperature ($1/T$), and the slope and intercept values were obtained as −2725.5 and −5.707, respectively. Thus, the activation energy (E_a) and frequency factor (A) of Cd volatilization can be calculated as 22.66 kJ mol^{-1} and 0.047 min^{-1}, respectively. The fitted models of Cd volatilization for Cl-LWAs-0 were established and are shown in eqn (8).

$$H = 1 - \exp\left(-0.047 \exp\left(-\frac{2725.5}{T}\right)t\right) \quad (8)$$

Similarly, the Cd volatilization rate of Cl-LWAs-0.8, the S-LWAs-0 and S-LWAs-0.8 were also measured and fitted using the same fitting process. The main factor values of the fitted models are listed in Table 1.

The corresponding kinetic models for the reactions of Cl-LWAs-0.8, S-LWAs-0 and S-LWAs-0.8 are shown as eqn (9)–(11), and the specific experimental parameters are shown in Fig. S3–S5† and are listed in Table S4–S6.†

$$H_{\text{Cl-LWA-0.8}} = 1 - \exp\left(-0.6027 \exp\left(-\frac{5960}{T}\right)t\right) \quad (9)$$

$$H_{\text{S-LWAs-0}} = 1 - \exp\left(-0.1585 \exp\left(-\frac{3998.7}{T}\right)t\right) \quad (10)$$

$$H_{\text{S-LWAs-0.8}} = 1 - \exp\left(-0.3717 \exp\left(-\frac{5126.3}{T}\right)t\right) \quad (11)$$

According to the results of the Cd volatilization kinetic models described above, it was found that the CaO might increase the activation energy required (E_a) for Cd volatilization at high temperatures and decrease the Cd volatilization rate. To verify the accuracy of the kinetic models to predict Cd volatility, we compared the experimentally obtained Cd volatilization rate with the model-predicted Cd volatilization rate at a sintering temperature of 1150 °C for a holding time of 30 min. For Cl-LWAs-0, the experimentally observed Cd volatilization rate was 18.22%, and the Cd volatilization rate predicted by the kinetic model was 18.76%, the error was only 0.54%, which

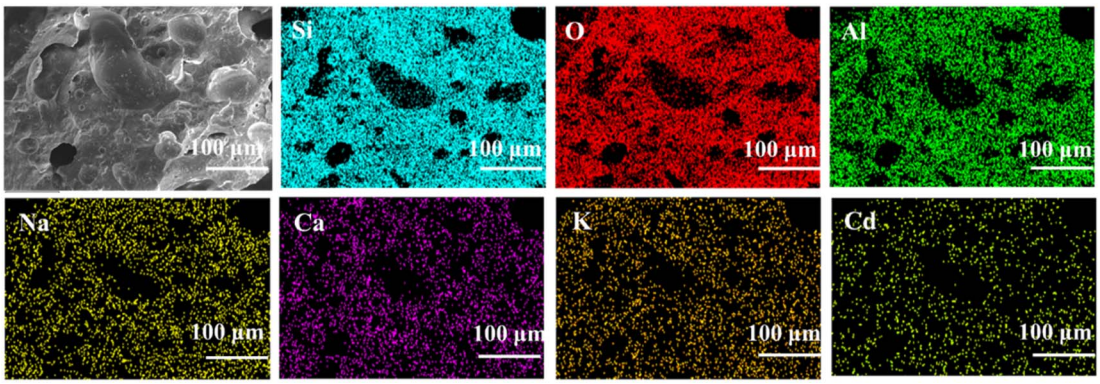

Fig. 6 The SEM image and the corresponding EDS mapping of the elements in S-LWA-0.8.

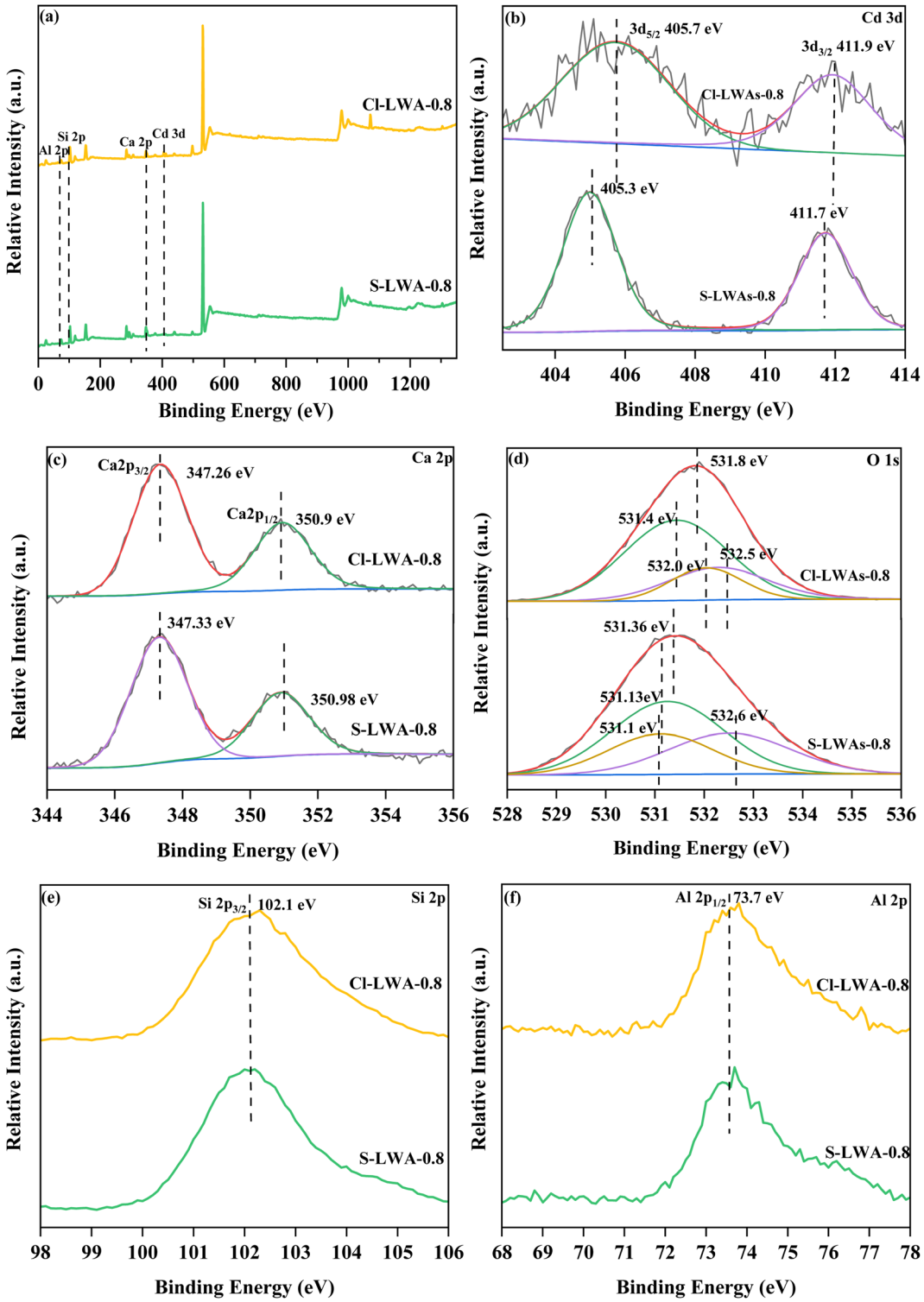

Fig. 7 XPS spectra of Cl-LWA-0.8 and S-LWA-0.8. (a) Survey spectrum, (b) Cd 3d, (c) Ca 2p, (d) O 1s (e) Si 2p and (f) Al 2p.

indicates that the established reaction kinetics model can effectively predict the Cd volatilization rate. Moreover, the error of the predicted Cd volatilization rates for Cl-LWAs-0.8, S-LWAs-0 and S-LWAs-0.8 were 0.07%, 0.03%, and 0.12%, respectively. The small error values between the theoretical and experimental volatilization rate also indicated that the fitted reaction kinetics model can better predict the Cd volatilization rate.

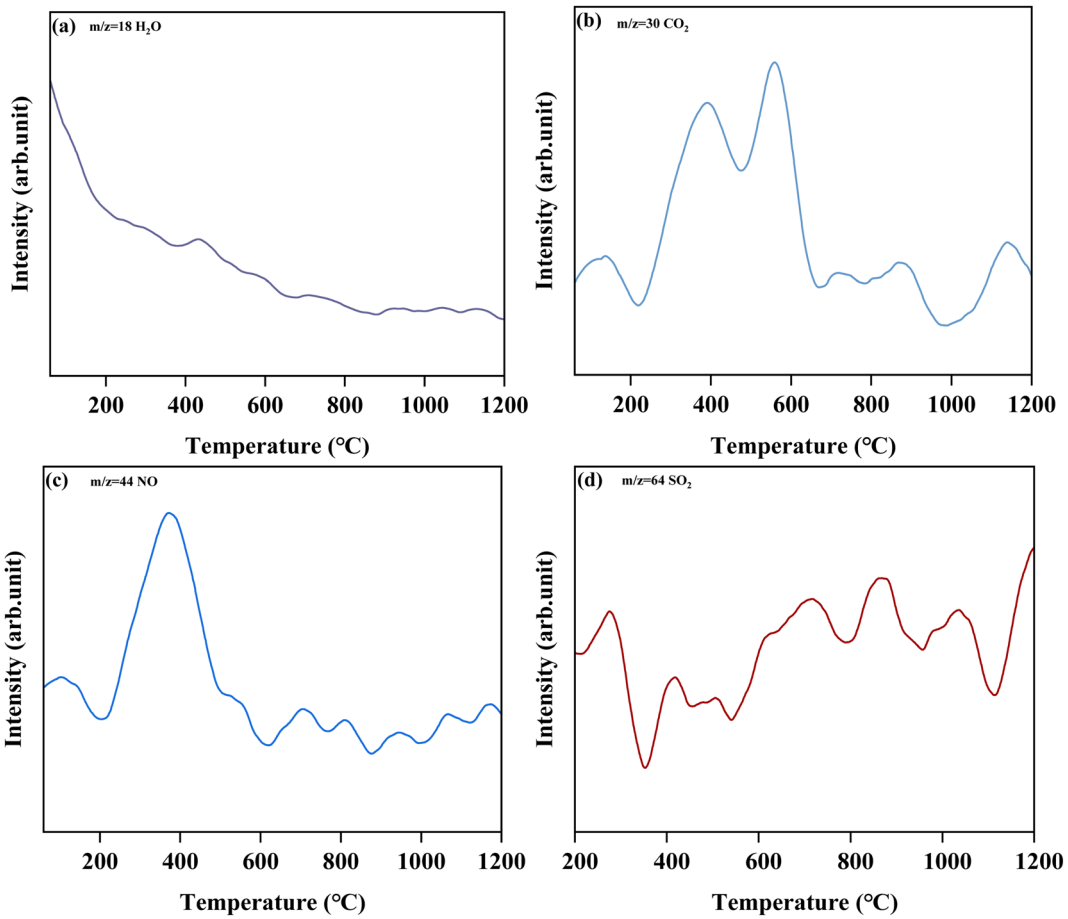

Fig. 8 Gas emission curves obtained during the high-temperature sintering of Cl-LWAs-0.8.

3.4 Analysis of the Cd solidification ratio

The leaching concentration of the LWAs with different CaO contents were used to examine the Cd solidification ratio in the LWAs and the results are shown in Fig. 3. The leaching experiments were conducted according to national standards of the toxicity characteristic leaching procedure (TCLP). It is evident that the Cd leaching concentration in both the Cl-LWAs-*x* and S-LWAs-*x* was lower than the limited values, and the solidification ratios of the residual Cd are all reach over 99.9%. Based on the leaching results, it was found that the CaO has a better solidifying effect on Cd under chlorine-containing conditions, which may be related to the different chemical reactions that occur between CaO and the added KCl and Na_2SO_4. This is probably because Ca^{2+} has a smaller atomic radius than K^+ which can

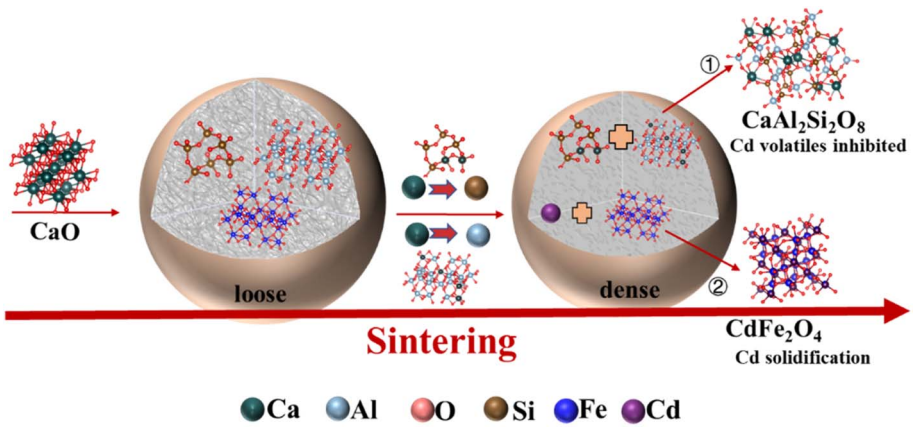

Fig. 9 Possible mechanism by which CaO affects Cd solidification.

react more readily with Cl^- first *via* a strong electron binding force. Moreover, volatile Cd is always produced at high temperatures above 600 °C, which usually volatilizes in the form of $CdCl_2$ and CdO.[43] Thus, the obvious decrease of Cd volatilization might be due to the CaO reacting with KCl to generate $CaCl_2$, which consumes Cl^- resulting in a decrease in the generation of volatile $CdCl_2$. However, CaO is slightly worse at controlling Cd volatilization in Na_2SO_4 containing LWAs. This might be due to the fact that Ca^{2+} has an ionic radius closely matched to Na^+, so the chemical effect of Ca^{2+} on Cd is similar to that of Na^+, which probably reduces CdO production at high temperatures with $SO_4{}^{2-}$. The results of the comparison of the Cd solidification properties in different solid waste-based material systems are shown in Table S11,† and also indicate that, in this study, CaO imparts an excellent solidification effect on Cd.

3.5 Mechanism analysis

3.5.1 XRD results. In order to determine the solidified forms of Cd that react with CaO, XRD was carried out on the mineral phases of the LWAs. As shown in Fig. 4, the main mineral phases in the LWAs with added CaO include quartz (SiO_2, PDF#99-0088), hematite (Fe_2O_3, PDF#85-0987), anorthite ($CaAl_2Si_2O_8$, PDF#20-0452) and cadmium spinel ($CdFe_2O_4$, PDF#22-1063). Both in the Cl-LWAs and S-LWAs, the results show that $CdFe_2O_4$ is the main product after the solidification of Cd. In Fig. 4(b) and (d), the diffraction peaks in the range from 35.2 to 36.4° are amplified. The formation of $CdFe_2O_4$ is considered to occur *via* the formation of Cd in the liquid state under solid confinement by disrupting the Si–O tetrahedral/Al–O octahedral structure and an amorphous phase is formed by replacing the Fe ions in the hematite.[44–46] The peak intensities of $CdFe_2O_4$ and $CaAl_2Si_2O_8$ increased with an increase in the CaO contents, and this may be the result of CaO promoting the disruption of the Si–O/Al–O structure to generate $CaAl_2Si_2O_8$ and accelerating the stable encapsulation of Cd^{2+} within the hematite. This finding is also consistent with the results of previous studies on the main product phase of Cd reactions at high temperature.[44,47] As one of the sources of skeleton strength structure, the $CaAl_2Si_2O_8$ might be the main product that improves the physical properties of the LWAs.[48,49]

3.5.2 Morphological analysis. For further observation of the internal structural distribution after the solidification of Cd, SEM images and EDS surface scans of typical areas of each of the LWAs were analyzed. For Cl-LWAs-0 and S-LWAs-0, the pore sizes were generally higher than 200 μm (Fig. S6(a) and S6(b)†), and the distribution of the pores on the matrix structure were uniform. After the addition of CaO, the large pore structures with pore sizes greater than 200 μm in Cl-LWAs-0.8 disappeared (Fig. S6(c) and S6(d)†). The significantly smaller number of large pores might be due to the addition of CaO, which can create good expansion of the LWAs during sintering and increase the connected liquid phase to convert large pores to small pores.[50,51] However, the pore structures in S-LWAs-0.8 (Fig. S6(e) and S6(f)†) are similar to those of S-LWAs-0, and the results showed that the regulated treatment of CaO has less of an effect under the influence of Na_2SO_4.

The EDS mapping results of Cl-LWAs-0.8 and S-LWAs-0.8 were compared to analyze the difference in structures.[52–54] As is shown in Fig. 5 and 6, the main elements of the LWAs are Si, O, Al, Na, K, and Ca, whilst the uniform distribution of Ca, O, Si and Al might indicate the presence of anorthite in the LWAs. Additionally, the EDS mapping and the estimated Cd content in the LWAs (Fig. 5) were summarized and the Cd mass content in Cl-LWAs-0.8 (Table S8†) is 0.5% while in Cl-LWA-0, the Cd content is only 0.08% (Table S7†). In S-LWA-0.8 (Fig. 6 and Table S10†), the quantity of Cd is 1.41% which is 0.52% higher than that of S-LWAs-0 (Table S9†). The increased Cd content indicates that CaO can effectively solidify the Cd and reduce the amount of volatile Cd present. According to the mapping results, the distribution of the elements including Si, Al, O, Na, Ca and Cd in S-LWAs-0.8 (Fig. 6) have a stronger signal than in Cl-LWAs-0.8, indicating that the Cd is better solidified, which was also consistent with the observation of a lower Cd(II) volatilization rate in S-LWAs-*x*.

3.5.3 XPS analysis. To better understand the changes of the chemical states after the CaO addition, the XPS spectra of Cl-LWA-0.8 and S-LWA-0.8 are displayed in Fig. 7. From the survey spectrum (Fig. 7(a)), the main elements including Cd, Ca, O, Si and Al in the LWAs can be seen. In Fig. 7(b), there are two characteristic peaks at 405.3–405.7 eV and 411.7–411.9 eV which might correspond to the spectra of Cd $3d_{5/2}$ and Cd $3d_{3/2}$, respectively, and indicate that the valence state of the Cd in the LWAs is only +2. The lower binding energy of the residual Cd in S-LWA-0.8 was identified, indicating that the Cd has a higher electronegativity and surface electron density in S-LWAs-0.8. The two characteristic peaks with binding energies at 347.26–347.33 eV and 350.9–350.98 eV correspond to Ca $2p_{3/2}$ and Ca $2p_{1/2}$, respectively, and the binding energy of Ca 2p in S-LWAs-0.8 is 0.09 eV higher than that of Cl-LWAs-0.8 (Fig. 7(c)). This may be due to S^{2-} having a larger ionic radius than Cl^- to interact with Ca^{2+} and enhance the binding energy. In the O 1s spectrum, the binding energies at 531.1–531.8 eV and 532.5–532.6 eV corresponded to the C=O and C–O–C bonds, respectively. In addition, there was no significant change in the XPS spectrum of Si 2p and Al 2p (Fig. 7(e) and (f)), implying that the effect of the solidified Cd in the LWAs on Si–Al compounds was small. This finding might be consistent with the stable amorphous crystal structure of $CaAl_2Si_2O_8$ in the LWAs. The lower binding energies of Cd 3d and O1s, but the higher binding energy of Ca^{2+} also indicate that the addition of CaO in S-LWAs-0.8 promotes Cd solidification *via* electronegative conversion.

3.5.4 TG-MS analysis. Fig. 8 shows the results of the TG-MS analysis used to detect the gas volatilization during the sintering of Cl-LWAs-0.8, which are used to analyze the possible mechanism of Cd volatilization. The gases detected in the sintering process mainly include H_2O, CO_2, NO and SO_2. By referring to previous TG-MS results of a blank sample,[26,27] the release of CO_2 and NO at 200–400 °C was caused by the decomposition of organic matter in contaminated soil, and the NO released at 400–700 °C was related to the thermal decomposition of mirabilite. Additionally, the SO_2 might be released

from the LS. The relatively low volatilization of SO_2 and NO indicates the stability of the structures of the oxygenated substances after CaO addition. According to the results of dynamic models and CaO regulated experiments, it is found that CaO addition can effectively reduce the volatilization of Cd, and better improve the mechanical properties of the LWAs. Based on the analysis of the microscopic morphology and phase composition, it is inferred that the CaO has a fluxing and cationic effect that can break the Si–O/Al–O bonds and promote the dissolution of Cd in Fe_2O_3 instead of volatilization. This implies that the control that CaO exerts on Cd solidification mainly includes two possible reactions that generate $CaAl_2Si_2O_8$ by reaction with Al_2O_3 and SiO_2, thus improving the structural strength of the LWAs and strengthening the formation of the $CdFe_2O_4$ generated from Cd and Fe_2O_3 (Fig. 9).

4 Conclusions

This study elucidates the effect that the addition of different quantities of CaO has on Cd solidification in the LWA sintering process by establishing a kinetic model; the main conclusions can be summarized as follows.

(1) After addition of CaO, the Cd volatilization rate reduced from 84.9 to 12.64%, corresponding to an increase in the E_a from 22.62 to 49.55 kJ mol^{-1} under the influence of chlorine, while the Cd volatilization rate under the influence of sulfate was reduced from 30 to 8%, with an increase in the E_a from 33.25 to 42.62 kJ mol^{-1}.

(2) CaO can effectively solidify Cd by optimizing the pore structure and improving the density, thus resulting in a solidification ratio of greater than 99.9%. The CaO also can work as a flux component to promote the generation of $CaAl_2Si_2O_8$.

(3) The solidification of Cd promoted by CaO is mostly due to the breaking of Si–O/Al–O bonds at high temperatures through the influence of its cationic properties, which also accelerate the stable encapsulation of Cd^{2+} within hematite to solidify the Cd of $CdFe_2O_4$ in the LWAs.

Data availability

Data will be made available on request.

Author contributions

Xin Gao: conceptualization, methodology, formal analysis, investigation, data curation, and writing original draft. Shouwei Jian: conceptualization, software, validation, writing – review & editing, resources, funding support, and project administration. Yuting Lei: validation, investigation, methodology, writing – review & editing. Baodong Li: formal analysis, methodology, and investigation. Jianxiang Huang: investigation, writing – review & editing. Xiaoyao Ma: investigation, validation, writing – review & editing. Xinxin He: investigation, writing – review & editing.

Conflicts of interest

The authors declare that they have no known competing financial interests or personal relationships that could have appeared to influence the work reported in this paper.

Acknowledgements

This work was supported by National Natural Science Foundation of China (No. 52178250) and Key Research and Development Plan of Hubei Province, China (2021BCA153).

References

1 N. Jordanova, D. Jordanova, E. Tcherkezova, B. Georgieva and D. Ishlyamski, *Sci. Total Environ.*, 2021, **792**, 148402.
2 M. A. S. Laidlaw, G. M. Filippelli, S. Brown, J. Paz-Ferreiro, S. M. Reichman, P. Netherway, A. Truskewycz, A. S. Ball and H. W. Mielke, *Appl. Geochem.*, 2017, **83**, 14–30.
3 S. Rebello, A. N. Anoopkumar, E. M. Aneesh, R. Sindhu, P. Binod, S. H. Kim and A. Pandey, *J. Hazard. Mater.*, 2021, **402**, 123474.
4 Y. A. Kumar, G. Mani, M. R. Pallavolu, S. Sambasivam, R. R. Nallapureddy, M. Selvaraj, M. Alfakeer, A. A. A. Bahajjaj, M. Ouladsmane, S. S. Rao and S. Ramakrishna, *J. Colloid Interface Sci.*, 2022, **609**, 434–446.
5 N. Sarwar, M. Imran, M. R. Shaheen, W. Ishaque, M. A. Kamran, A. Matloob, A. Rehim and S. Hussain, *Chemosphere*, 2017, **171**, 710–721.
6 J. Rinklebe, S. M. Shaheen, A. El-Naggar, H. Wang, G. Du Laing, D. S. Alessi and Y. Sik Ok, *Environ. Int.*, 2020, **140**, 105754.
7 S. Wang, L.-M. Cai, H.-H. Wen, J. Luo, Q.-S. Wang and X. Liu, *Sci. Total Environ.*, 2019, **655**, 92–101.
8 H. Zhao, X. Huang, F. Liu, X. Hu, X. Zhao, L. Wang, P. Gao, X. Li and P. Ji, *Environ. Pollut.*, 2021, **269**, 116198.
9 B. Zhang, Y. Cheng, J. Shi, X. Xing, Y. Zhu, N. Xu, J. Xia and A. G. L. Borthwick, *Chem. Eng. J.*, 2019, **375**, 121965.
10 L.-M. Cai, Q.-S. Wang, J. Luo, L.-G. Chen, R.-L. Zhu, S. Wang and C.-H. Tang, *Sci. Total Environ.*, 2019, **650**, 725–733.
11 M. Komárek, A. Vaněk and V. Ettler, *Environ. Pollut.*, 2013, **172**, 9–22.
12 Y. He, D. Huang, Q. Zhu, S. Wang, S. Liu, H. He, H. Zhu and C. Xu, *Ecotoxicol. Environ. Saf.*, 2017, **136**, 135–141.
13 M. Moniruzzaman, Y. Anil Kumar, M. R. Pallavolu, H. M. Arbi, S. Alzahmi and I. M. Obaidat, *Nanomaterials*, 2022, **12**, 3187.
14 B. González-Corrochano, J. Alonso-Azcárate and M. Rodas, *Constr. Build. Mater.*, 2012, **35**, 497–507.
15 B. Li, S. Jian, J. Zhu, H. Yu, R. Wu, W. Gao and H. Tan, *Waste Manage.*, 2020, **118**, 131–138.
16 M. J. Quina, M. A. Almeida, R. Santos, J. M. Bordado and R. M. Quinta-Ferreira, *Appl. Clay Sci.*, 2014, **102**, 71–80.
17 Y. Shao, Y. Shao, W. Zhang, Y. Zhu, T. Dou, L. Chu and Z. Liu, *Waste Manage.*, 2022, **143**, 54–60.
18 J. Pei, X. Pan, Y. Wang, Z. Lv, H. Yu and G. Tu, *Ceram. Int.*, 2023, **49**, 18379–18387.

19 R. Zhao, B. Wang, B. K. G. Theng, P. Wu, F. Liu, X. Lee, M. Chen and J. Sun, *Sci. Total Environ.*, 2021, **799**, 149295.
20 G. Xu, M. Liu and G. Li, *J. Hazard. Mater.*, 2013, **260**, 74–81.
21 E. M. Kalhori, K. Yetilmezsoy, N. Uygur, M. Zarrabi and R. M. A. Shmeis, *Appl. Surf. Sci.*, 2013, **287**, 428–442.
22 J.-H. Yoon, Y. A. Kumar, S. Sambasivam, S. A. Hira, T. N. V. Krishna, K. Zeb, W. Uddin, K. D. Kumar, I. M. Obaidat, S. Kim and H.-J. Kim, *J. Energy Storage*, 2020, **32**, 101988.
23 Z. Wang, W. Yang, H. Liu, H. Jin, H. Chen, K. Su, Y. Tu and W. Wang, *J. Anal. Appl. Pyrolysis*, 2019, **142**, 104617.
24 B. Zhang, A. Bogush, J. Wei, T. Zhang, W. Xu and Q. Yu, *Constr. Build. Mater.*, 2018, **182**, 144–155.
25 Y. Zhang, Y. Chen, A. Meng, Q. Li and H. Cheng, *J. Hazard. Mater.*, 2008, **153**, 309–319.
26 S. Jian, Y. Lei, B. Li, X. Li, H. Tan, J. Huang, Y. Lv and W. Gao, *Ceram. Int.*, 2022, **48**, 19283–19294.
27 S. Jian, Y. Lei, B. Li, Y. Lv, X. Gao and X. Yang, *Constr. Build. Mater.*, 2022, **352**, 129041.
28 J.-z. Luo, B.-x. Sheng and Q.-q. Shi, *J. Fuel Chem. Technol.*, 2020, **48**, 1318–1326.
29 D. J. Lane, J. Jokiniemi, M. Heimonen, S. Peräniemi, N. M. Kinnunen, H. Koponen, A. Lähde, T. Karhunen, T. Nivajärvi, N. Shurpali and O. Sippula, *Waste Manage.*, 2020, **114**, 1–16.
30 Z. Zhang, M. Zhao, Y. Zhang, C. Liu, W. Zhu, G. Liu, Y. Yang, G. Sun and L. Yang, *Ceram. Int.*, 2023, **49**, 28326–28336.
31 B. Nowak, S. Frías Rocha, P. Aschenbrenner, H. Rechberger and F. Winter, *Chem. Eng. J.*, 2012, **179**, 178–185.
32 S.-J. Wang, H. Zhang, L.-M. Shao, S.-M. Liu and P.-J. He, *Chemosphere*, 2014, **117**, 353–359.
33 Y. Du, X. Wang, X. Ji, Z. Zhang, U. K. Saha, W. Xie, Y. Xie, J. Wu, B. Peng and C. Tan, *Chemosphere*, 2018, **204**, 130–139.
34 Y. Long, Y. Song, Y. Yang, H. Huang, H. Fang, D. Shen, H. Geng, J. Ruan and F. Gu, *J. Environ. Manage.*, 2023, **338**, 117776.
35 D. Perondi, D. Restelatto, C. Manera, M. Godinho, A. J. Zattera and A. C. Faria Vilela, *Process Saf. Environ. Prot.*, 2019, **122**, 58–67.
36 C. Xie, J. Liu, J. Liang, W. Xie, F. Evrendilek and W. Li, *Sci. Total Environ.*, 2021, **785**, 147219.
37 J. Jiang, S. Chen, C. Jin, G. Wang, T. Liu, T. Xu, L. Lei, W. Dang, X. Yang, T. Ding, Z. Li, Z. Lu and J. Li, *Constr. Build. Mater.*, 2023, **368**, 130458.
38 R. F. K. Gunnewiek and R. H. G. A. Kiminami, *Ceram. Int.*, 2014, **40**, 10667–10675.
39 A. K. Yedluri and H.-J. Kim, *Dalton Trans.*, 2018, **47**, 15545–15554.
40 D. K. Kulurumotlakatla, A. K. Yedluri and H.-J. Kim, *J. Energy Storage*, 2020, **31**, 101619.
41 Y. Anil Kumar and H.-J. Kim, *New J. Chem.*, 2018, **42**, 19971–19978.
42 C. F. Valdés, G. Marrugo, F. Chejne, J. D. Román and J. I. Montoya, *J. Anal. Appl. Pyrolysis*, 2016, **121**, 93–101.
43 J. Liu, Q. Falcoz, D. Gauthier, G. Flamant and C. Z. Zheng, *Chemosphere*, 2010, **80**, 241–247.
44 M. Su, J. Tang, C. Liao, L. Kong, T. Xiao, K. Shih, G. Song, D. Chen and H. Zhang, *Environ. Pollut.*, 2018, **239**, 571–578.
45 Y. Anil Kumar, S. Sambasivam, S. Ahmed Hira, K. Zeb, W. Uddin, T. N. V. Krishna, K. Dasha Kumar, I. M. Obaidat and H.-J. Kim, *Electrochim. Acta*, 2020, **364**, 137318.
46 H.-J. Kim, B. Naresh, I.-H. Cho, J.-S. Bak, S. A. Hira, P. R. Sekhar Reddy, T. N. V. Krishna, K. Dasha Kumar, B. A. Mola and Y. A. Kumar, *J. Energy Storage*, 2021, **40**, 102702.
47 M. H. Mahmoud, A. M. Abdallas, H. H. Hamdeh, W. M. Hikal, S. M. Taher and J. C. Ho, *J. Magn. Magn. Mater.*, 2003, **263**, 269–274.
48 N. de Koker, *Geochim. Cosmochim. Acta*, 2010, **74**, 5657–5671.
49 K. Inage, K. Akatsuka, K. Iwasaki, T. Nakanishi, K. Maeda and A. Yasumori, *J. Non-Cryst. Solids*, 2020, **534**, 119948.
50 Y. Anil Kumar, K. Dasha Kumar and H.-J. Kim, *Dalton Trans.*, 2020, **49**, 3622–3629.
51 Y. Anil Kumar, S. Singh, D. K. Kulurumotlakatla and H.-J. Kim, *New J. Chem.*, 2020, **44**, 522–529.
52 Y. A. Kumar, B. A. Al-Asbahi, M. R. Pallavolu, S. S. Rao, R. R. Nallapureddy and S. Ramakrishna, *Int. J. Energy Res.*, 2022, **46**, 14227–14239.
53 Y. A. Kumar, H. T. Das, P. R. Guddeti, R. R. Nallapureddy, M. R. Pallavolu, S. Alzahmi and I. M. Obaidat, *Nanomaterials*, 2022, **12**, 2330.
54 B. A. Mola, M. R. Pallavolu, B. A. Al-Asbahi, Y. Noh, S. K. Jilcha and Y. A. Kumar, *J. Energy Storage*, 2022, **51**, 104542.